Scanning Tunneling Microscopy

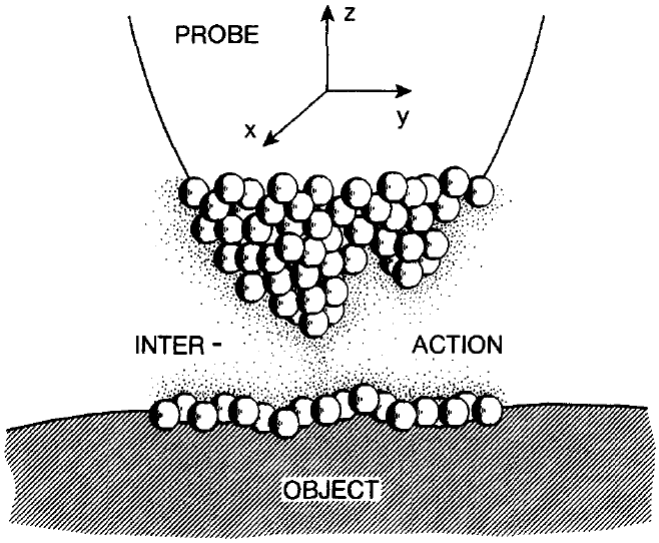


J.A. Kubby and J.J. Boland, Surf. Sci. Rep. **26** 61-204 (1996)

$$-(\hbar^2/2m)\psi'' + [V(x) - E]\psi = 0$$

has the solutions

$$\psi(x) = \begin{cases} Ae^{+ikx} + Be^{-ikx} & (x < 0), \\ Ce^{-kx} + De^{+kx} & (0 < x < s), \\ Fe^{+ikx} & (x < s), \end{cases}$$

where

$$\hbar k = (2mE)^{1/2}; \qquad \hbar \mathrm{k} = (2m[V_0 - E])^{1/2}.$$

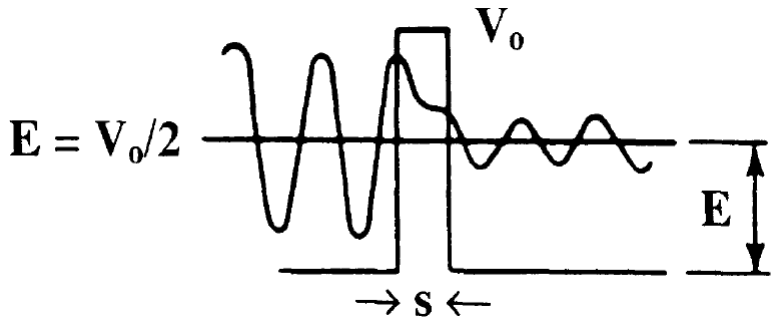
$V_0$
$E = V_0/2$
E
→ s ←

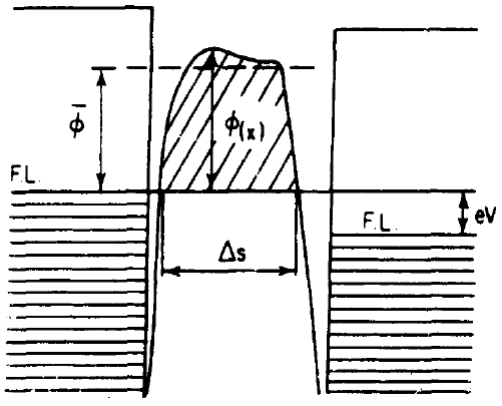
$\bar{\phi}$
$\phi_{(x)}$
F.L.
F.L.
eV
Δs

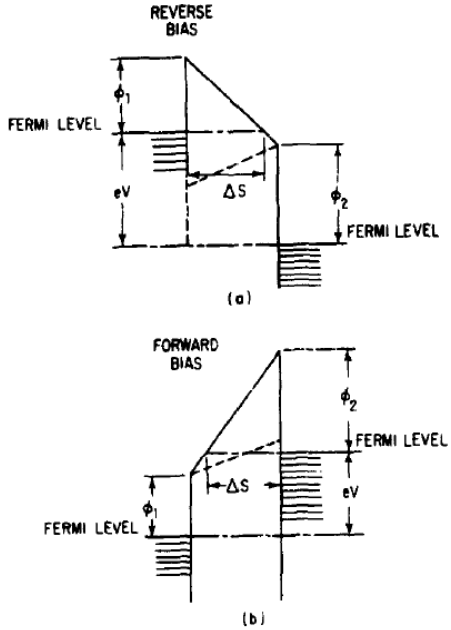
REVERSE
BIAS
$\phi_1$
FERMI LEVEL
eV
ΔS
$\phi_2$
FERMI LEVEL
(a)
FORWARD
BIAS
$\phi_2$
FERMI LEVEL
ΔS
eV
$\phi_1$
FERMI LEVEL
(b)

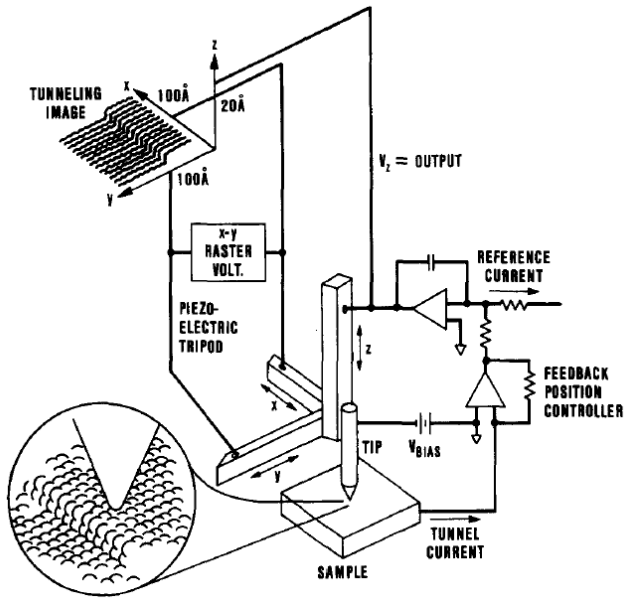
z
TUNNELING
IMAGE
x
100Å
20Å
100Å
y
$V_z$ = OUTPUT
x-y
RASTER
VOLT.
REFERENCE
CURRENT
PIEZO-
ELECTRIC
TRIPOD
z
FEEDBACK
POSITION
CONTROLLER
x
TIP
$V_{BIAS}$
y
TUNNEL
CURRENT
SAMPLE

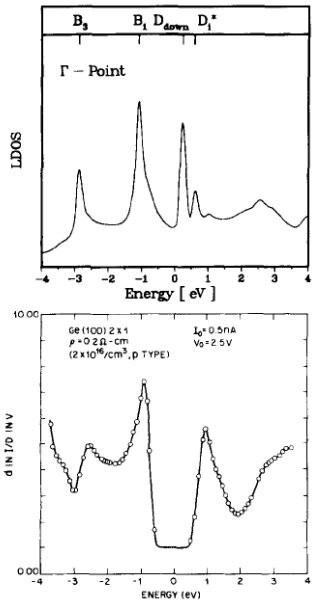


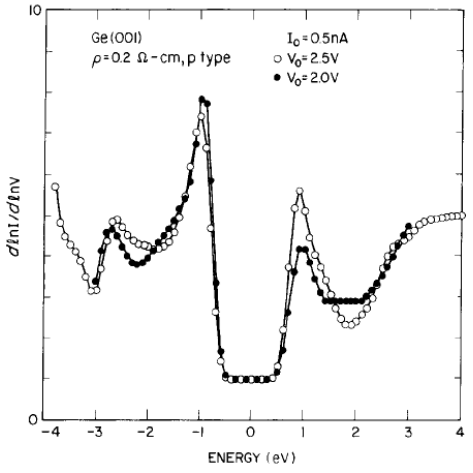


Fig. 82. Normalized conductance vs. bias voltage relative to the Fermi energy. Stabilization voltages of 2.0 and 2.5 V at a demanded tunneling current of 0.5 nA were used to obtain the spectra. The spectra shown are the average of 200 spectra. The occupied-state peak at $-1$ eV corresponds to the $D_{up}$ ($\pi$-bonding) band, and the unoccupied-state peak at $+0.9$ eV corresponds to the $D_{down}$ ($\pi^*$-anti-bonding) band. The energy scale is shown for sample bias [286].

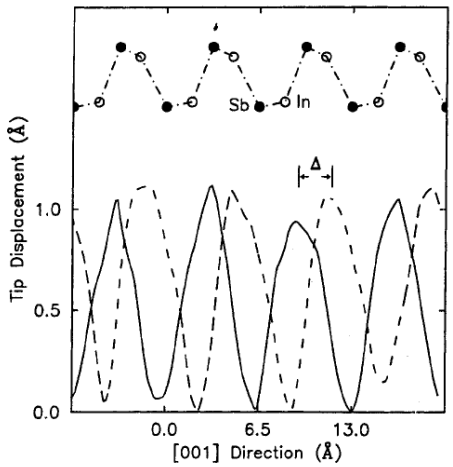


Fig. 111. A pair of STM profiles along the [0 0 1] direction of InSb(1 1 0) interpolated from two images acquired simultaneously at $-1.5$ V (solid line; antimony, filled states) and $+1.35$ V (dashed line; indium, empty states). The average displacement, $\Delta$, of the antimony and indium state density is $2.4 \pm 0.4$ Å. A side view of the atomic structure of the top two surface layers as calculated by Mailhiot et al. [370] is shown for comparison (vertical dimensions not to scale) [369].

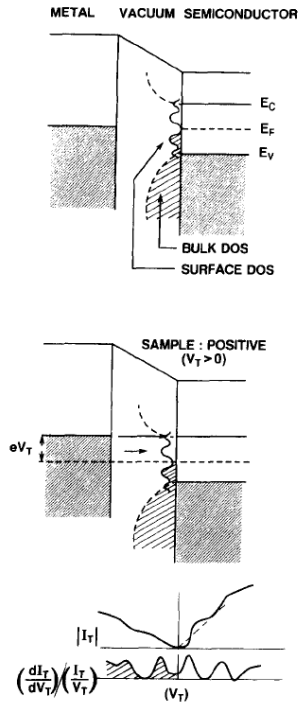

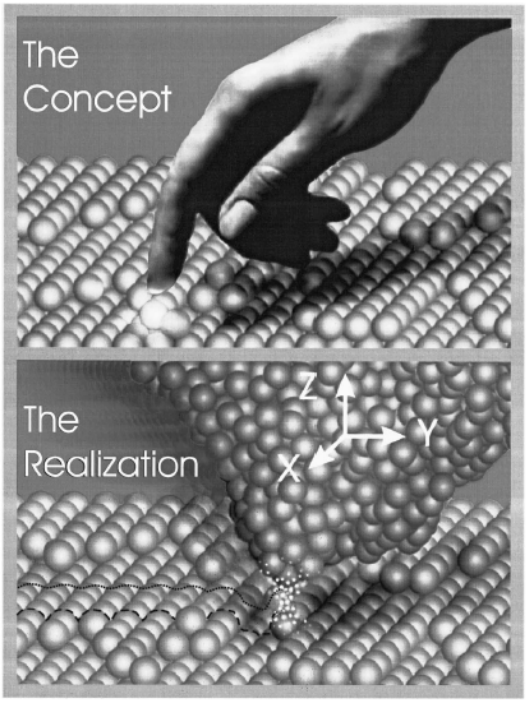
The
Concept
The
Realization
Z
Y
X

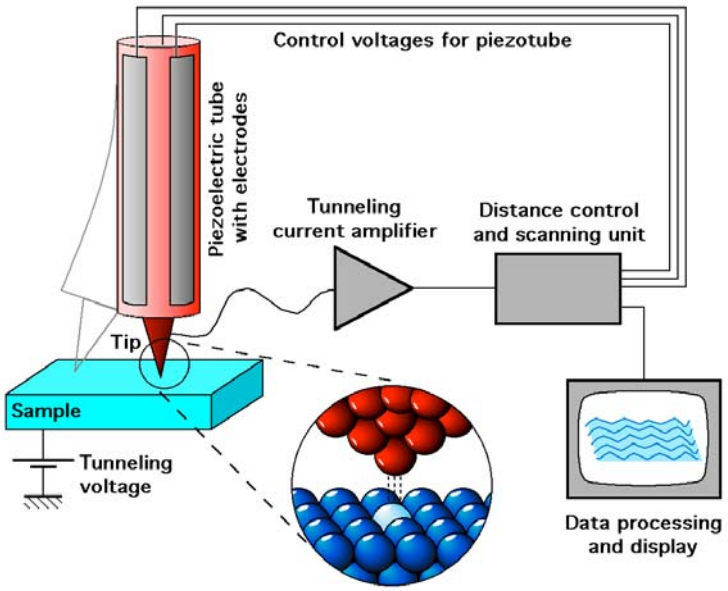
Control voltages for piezotube
Piezoelectric tube
with electrodes
Tunneling
current amplifier
Distance control
and scanning unit
Tip
Sample
Tunneling
voltage
Data processing
and display

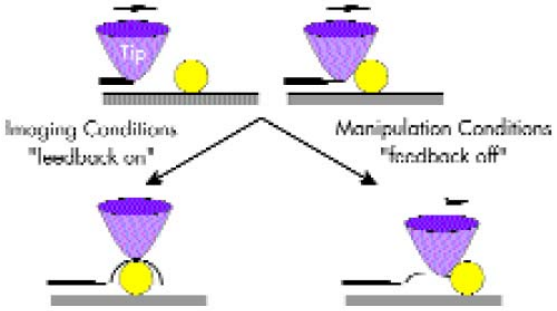


Figure 2. Imaging takes place with the feedback control on. Turning off the feedback allows the mechanical pushing of the nanoparticle.

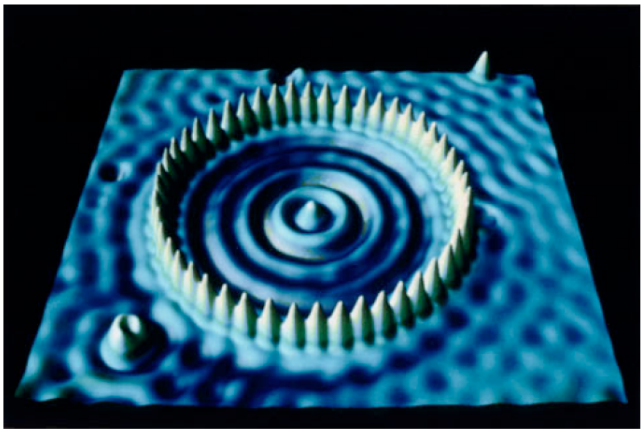

FIG. 2. (Color) STM image of a quantum corral for electrons built with 48 iron atoms on copper. The same tip is used to position the iron atoms into a 12.4-nm-diameter ring and to image them and the wave-structure interior caused by the confined surface-state copper electrons. Courtesy D. Eigler, IBM Research Center, Almaden, CA.

G. Binnig and H. Rohrer, Rev. Mod. Phys., Vol. 71, S324 (1999)

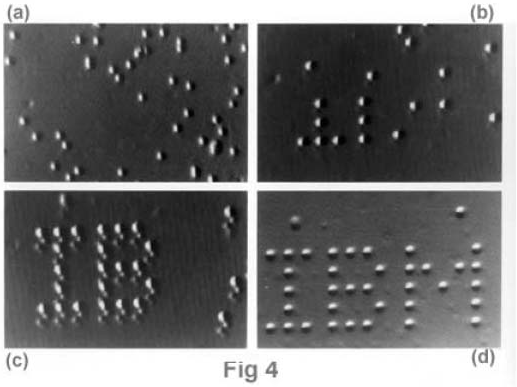


**Figure 4:** Work by D.M. Eigler and E.K. Schweizer, presented in Nature, vol 344, p. 524 (1990). A sequence of STM images taken during the construction of a patterned array of xenon atoms on a nickel surface at temperature 4 K. Xenon atoms were allowed to stick randomly on the surface from the gas phase (panel a), and then were moved one by one (panels b-f) to spell out the name of the company sponsoring the research. This image was provided by D. Eigler of IBM Almaden Research Laboratories.

Scanning Tunneling Microscopy, E.D. Williams, UMD

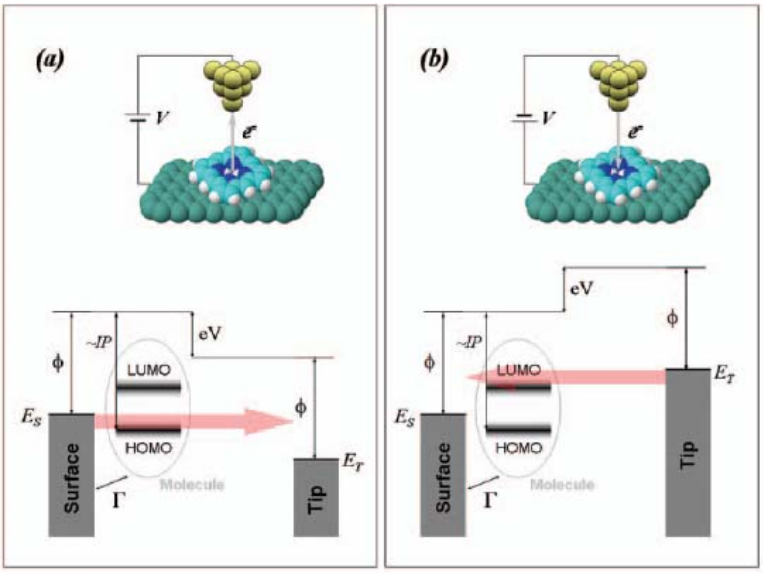


Figure 5. Energy diagram for an STM junction when applying a negative (a) or positive (b) sample bias. The position of molecular frontier orbitals (HOMO and LUMO) and Fermi levels of substrate ($E_S$) and tip ($E_T$) are indicated. While molecular energy levels are broadened and shifted due to electronic coupling ($\Gamma$) to substrate states (and other phenomena), their approximate position can be estimated by pinning the vacuum level of the isolated molecule to that of the substrate.

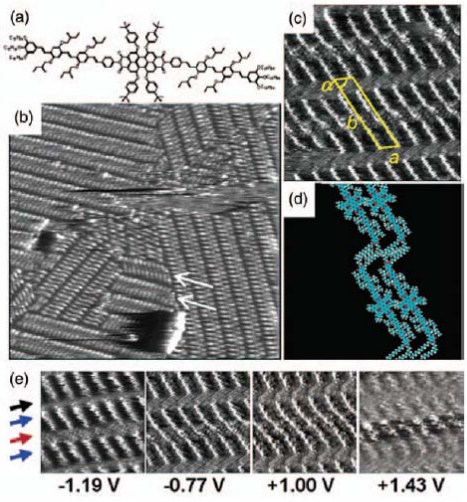


re 20. (a) Chemical structure of the D-A-D triad. (b) Constant height STM image 2nm X 70.2nm, sample bias –0.96V, 150pA tunneling current) of a D-A-D monolayer at the face between a 1-phenyloctane solution and the basal plane of graphite. Arrows indicate ork-image type packing. (c) High-resolution STM image (15.5nm X 15.5nm, sample bias '0V, 400pA tunneling current) with overlaid parallelogram indicating a monolayer unit cell. roposed molecular model reflecting the ordering in (c). (e) Bias-dependent imaging of the D triad (10.1nm X 10.1nm, 400pA tunneling current, sample bias indicated below each ge). In order top-to-bottom, the arrows on the left refer to alkyl chains, donor units, acceptor , and donor units. Reprinted with permission from Atsushi Miura, Zhijian Chen, Hiroshi Uji, en de Feyter, Magdalena Zdanowska, Pascal Jonkheijm, Albertus P. H. J. Schenning, E. W. er, Frank Würthner, and Frans C. de Schryver, J. Am. Chem. Soc., 2003, 125(49), 68-9. Copyright (2003) American Chemical Society.

Petri P. Lehenkari, Guillaume T. Charras, Stephen A. Nesbitt and Mike A. Horton, expert reviews in molecular medicine http://www-ermm.cbcu.cam.ac.uk (2000).

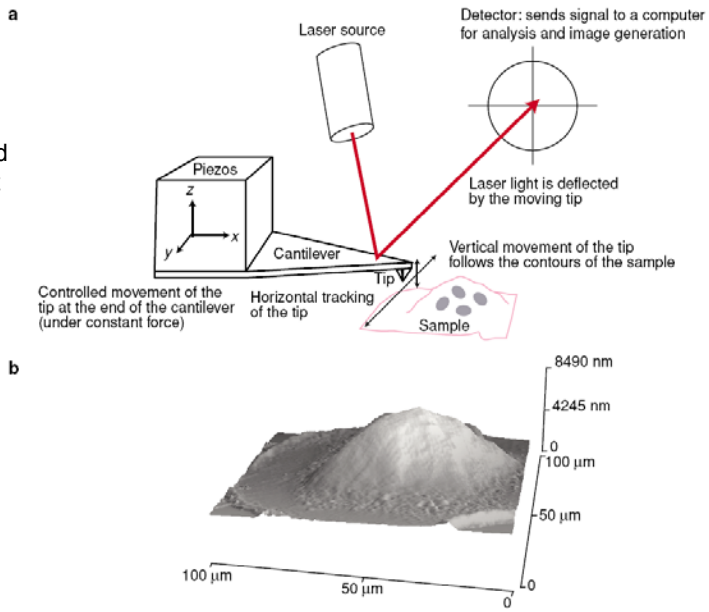


How the atomic force microscope scans surfaces

Expert Reviews in Molecular Medicine © 2000 Cambridge University Press

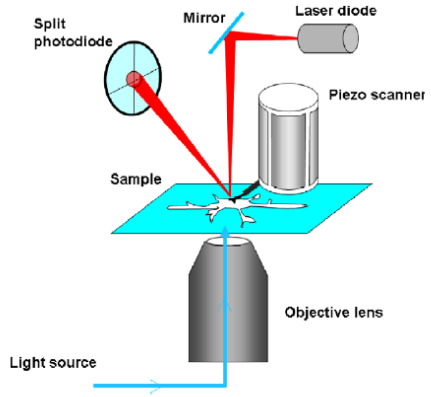


**Figure 1.** Scheme of an AFM coupled with an inverted optical microscope.

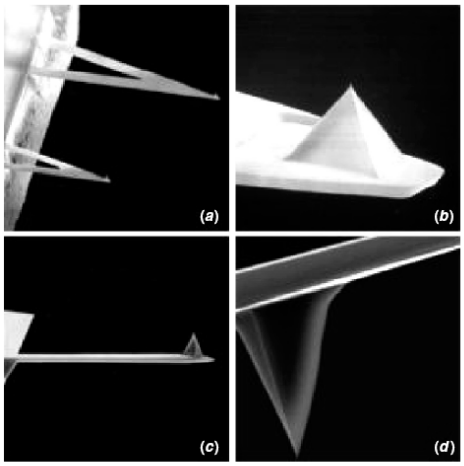


**Figure 2.** Scanning electron microscope images of microfabricated AFM cantilevers and tips. (*a*) Silicon nitride cantilevers and (*b*) high magnification of the tip with oxide-sharpened apex; (*c*) silicon cantilever and (*d*) high magnification of the silicon tip. Courtesy of Veeco Instruments.

interactions. At the end we will summarize the possible future trends in this field enumerating the most promising forthcoming technical developments and appealing scientific problems that could be faced using the AFM.

Andrea Alessandrini and Paolo Facci, Meas. Sci. Technol. 16 (2005) R65–R92
Online at stacks.iop.org/MST/16/R65

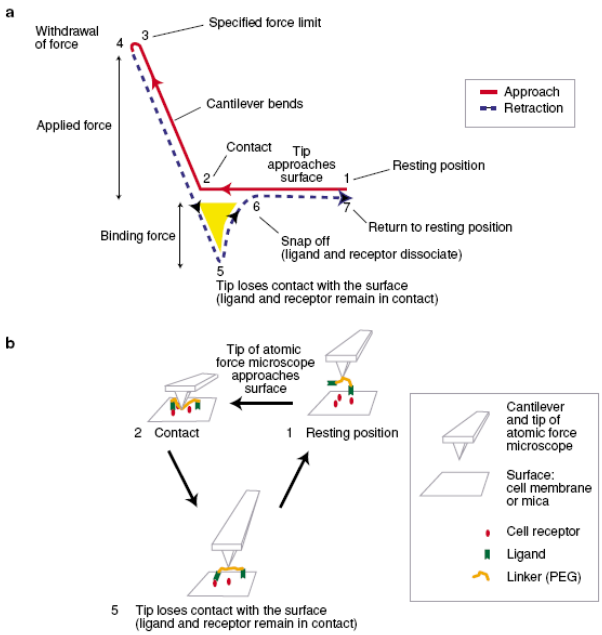


How the atomic force microscope generates force–distance curves for a cell receptor and ligand

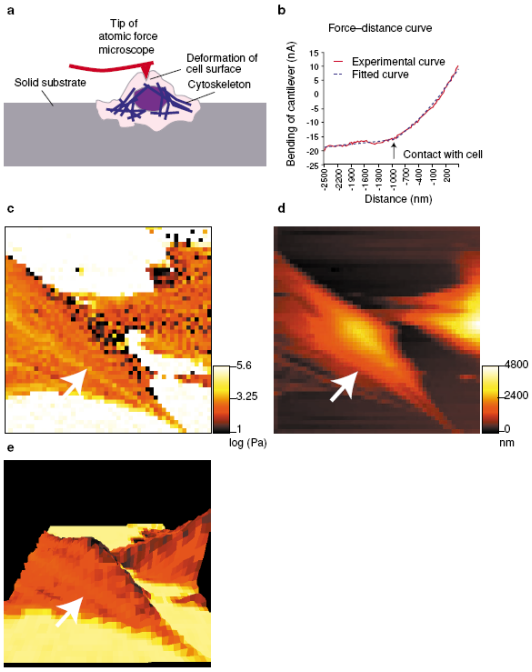


Examining the material properties of a cell using atomic force microscopy



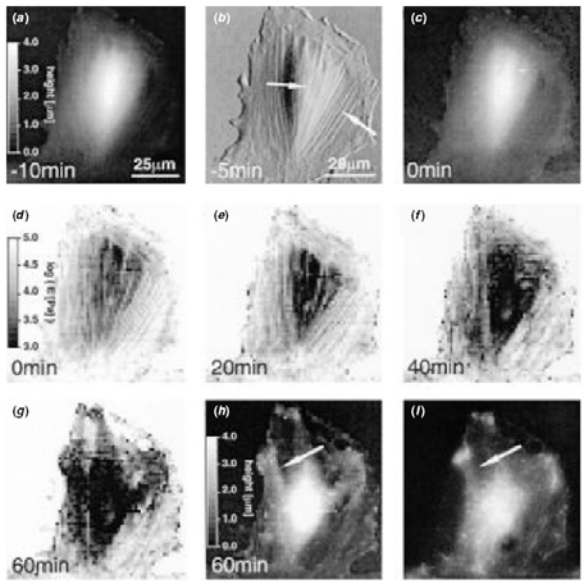


**Figure 19.** Time series of elasticity maps of an NRK fibroblast showing disaggregation of the actin network by 10 mM cytochalasin D and correlation with AFM and fluorescence images. (*a*) Contact AFM image. (*b*) AFM deflection image; stress fibres are depicted by arrows. (*c*) Height image at zero loading force calculated from the reference force map. (*d*) Corresponding reference elasticity map. (*e*), (*f*) Young's modulus decreases gradually within 40 min. (*g*) Elasticity map and (*h*) height image at zero loading force obtained after 60 min showing strong segmentation of the cytosol. (*i*) Corresponding fluorescence images to identify structures in (*g*) and (*h*) as clots of actin. The arrow in (*h*) points to a very flat region (500 nm) that correlates with a region devoid of f-actin (*i*, arrow). Reprinted with permission from [145]. 

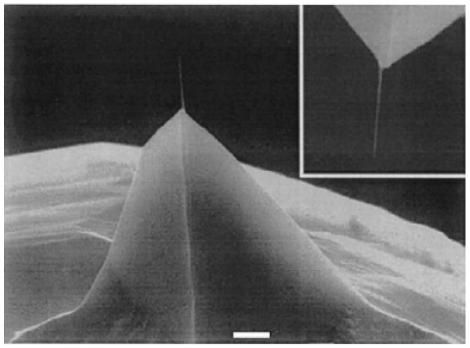

**Figure 3.** Multiwall carbon nanotube tip attached to the end of single-crystal silicon tip. The inset is a higher magnification view of the same tip rotated 180° relative to the main image (bar = 1 $\mu$m). Reprinted with permission from [22]. Copyright 1998, American Chemical Society.

tips is comparable with that of other ultimate resolution imaging techniques such as cryogenic electron microscopy, but carbon nanotubes offer also the possibility to be functionalized, exposing, thus, a well-defined chemical group or chemisorbed biomolecule. This opportunity can be exploited to study

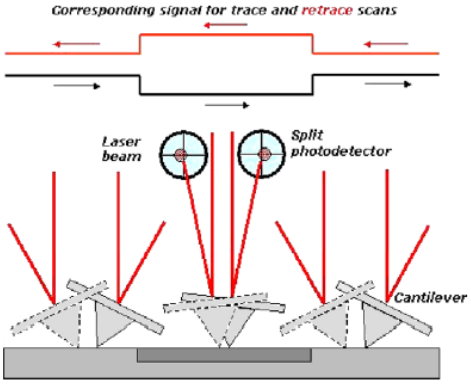


**Figure 4.** Operating principle of the lateral force mode. The signal from the lateral segments of the photodetector is monitored while the tip is scanned on the surface in the direction perpendicular to the major axis of the cantilever. Both the trace and retrace signals are recorded to avoid possible interference of the topographic signal with the lateral force signal. Indeed, a pure lateral force should give an inverted signal in the trace and retrace scan of the tip. Subtracting the two signals (trace and retrace) highlights the contrast coming only from lateral forces.

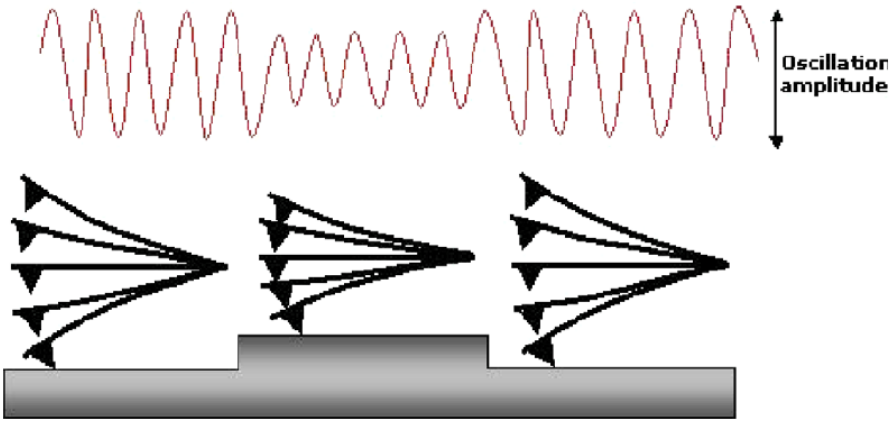


**Figure 5.** Schematic representation of an AFM tip operating in the intermittent contact mode.

No Dragging Forces

Less Damage to Soft Samples

(e.g., the NanoScope I
SPM controllers) have b

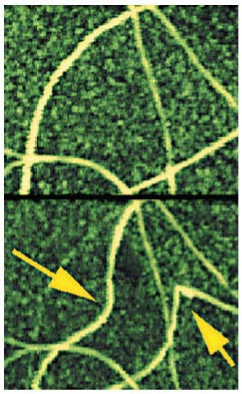

Figure 11a. AFM in-plane nanomanipulation uses the AFM probe to image, manipulate nanometer-scale objects (carbon nanotubes), and image again to see the results.

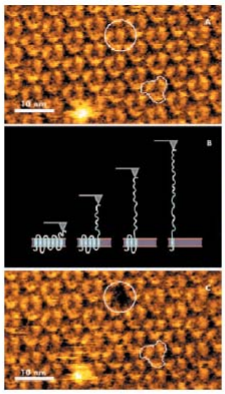

Figure 11b. AFM out-of-plane nanomanipulation uses the AFM probe to image, pull a single biomolecule out of the plane of the sample while measuring the unfolding of the molecule, and image again to see the results (in this case, the removal of one molecule from an array).

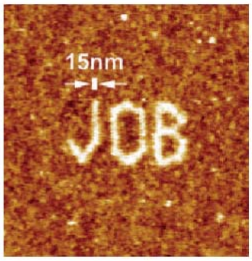


Figure 11c. AFM nanolithography.

Veeco website and application notes

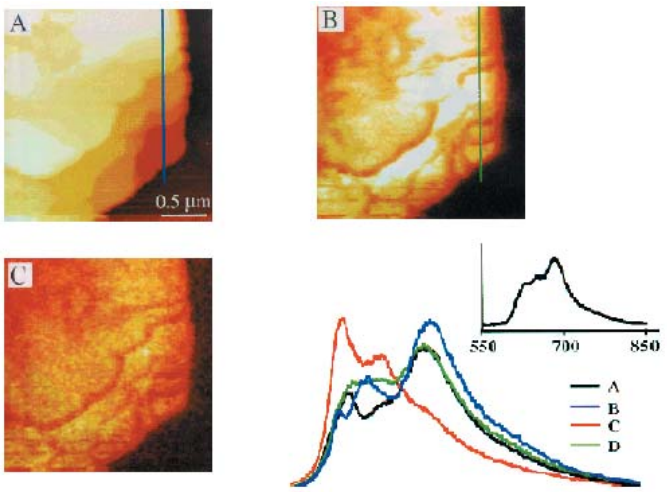


Figures 1. Topography and polarized fluorescence NSOM images of small PIC crystals excited at 514 nm. Image A is the topography of the crystal as measured by the shear force feedback of the NSOM. Images B and C are fluorscence NSOM images of the crystals polarized horizontally and vertically respectively. Image C is plotted on an intensity scale 5 times larger than B. The crystal is uniformly polarized with the fluorescence along the short axis being at least 5 times larger than from the long axis. The graph shows line scans across the topographic and horizontally polarized image. Note the dips in the fluorescence signal as the tip is scanned over the edges of the crystal plates. This is due to the sample leaving the near field of the excitation aperture as the tip is scanned over the edges of the crystal.

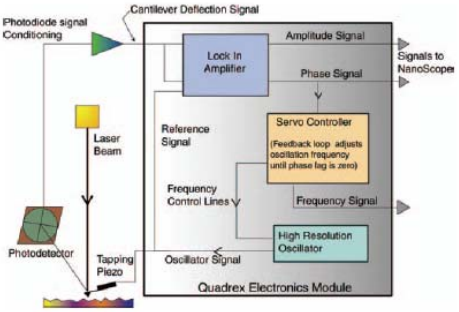


Figure 3a. Amplitude and phase detection and frequency modulation (FM) techniques for EFM.

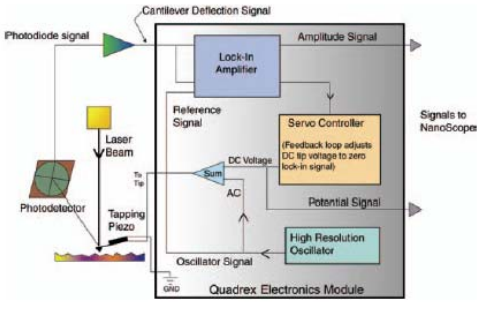


Figure 3b. Surface Potential (SP) Imaging.

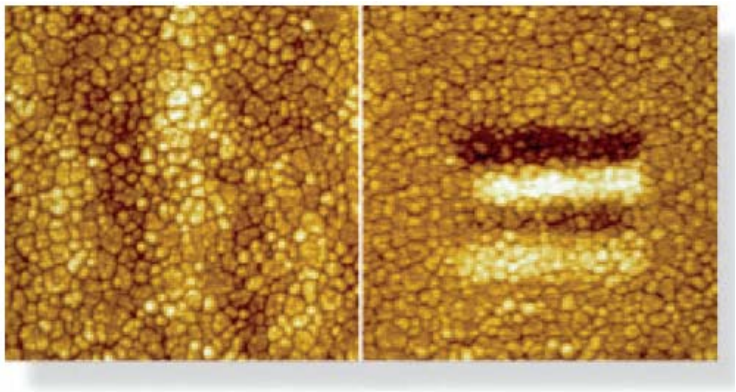

Figure 9. Topography (left) and FM-EFM (right) images of a ferroelectric film with electrical bits written onto it. The four bits were written with a metal-coated AFM tip at +3,-3,+2, and -2volts from top to bottom. The images were captured with the same tip, moments after polarizing the central region. Carrying +1V, the tip failed to polarize this ferroelectric film. 2μm scans.

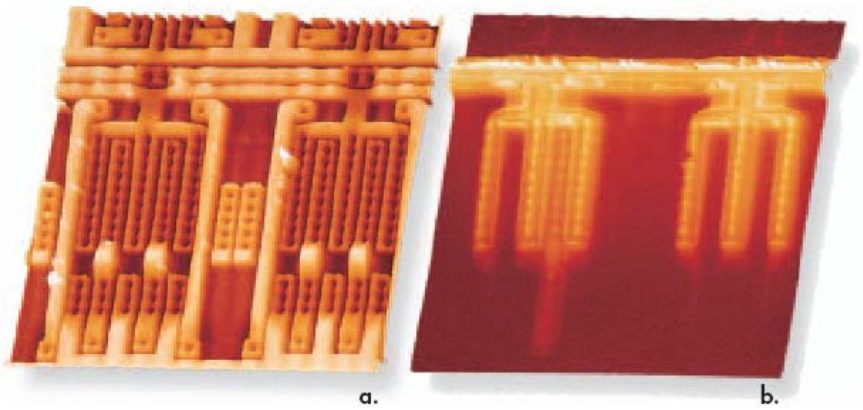


Figure 6. Topography (a) and EFM image (b) of a live packaged IC with passivation layer on. EFM image detects transistor in saturation. 80μm scans.

## The Physics and Applications of Self Assembled Quantum Dots

*M S Skolnick, Department of Physics, University of Sheffield*

1. Why self-assembled quantum dots (SAQDs) are important
2. Atom-like systems. Zero dimensional density of states
3. Enhanced exciton fine structure, long spin lifetimes
4. Coulomb interactions, coupling of 0D states to 2, 3D environment
5. Applications: ensembles, single dots
6. Conclusions, challenges

EPSRC

NanoMAT

## Modification of Density of States by Reduction of Dimensionality

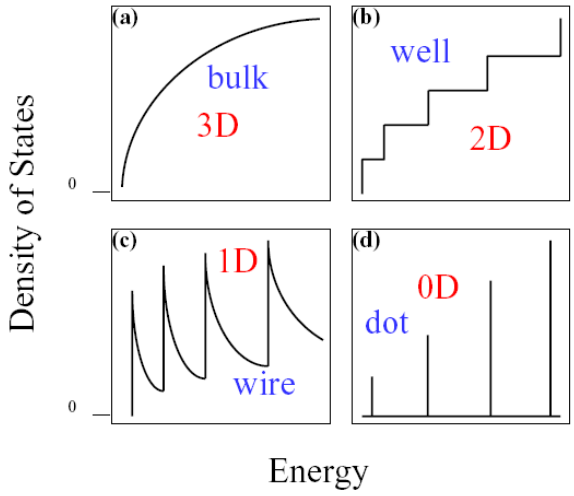


## Self-Assembled Crystal Growth in Strained Systems (schematic) MBE Growth

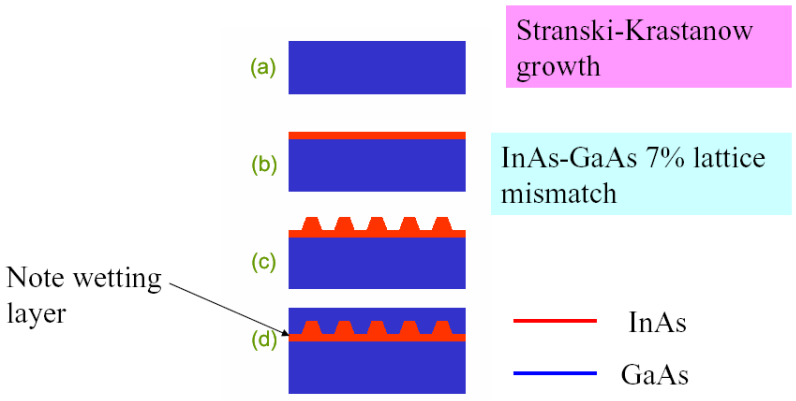


*Embedded in crystal matrix – like any other semiconductor laser or light emitting diode*

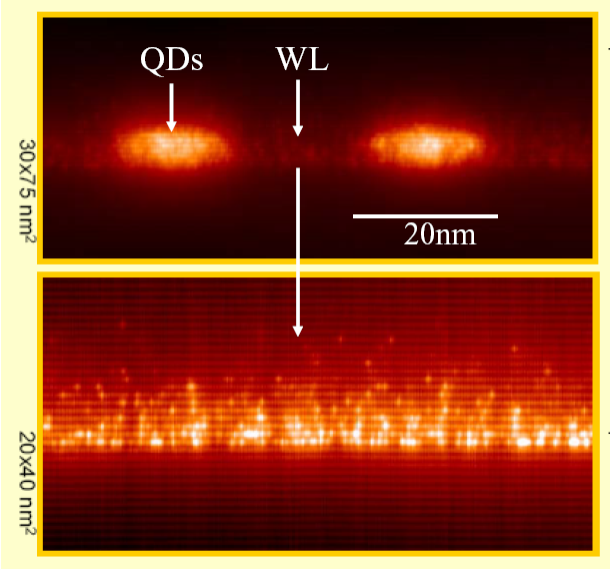


UHV-STM cross sections

PM Koenraad, TU Eindhoven

## •Energy Level Structure

- Discrete energy levels – atom-like
- Electron energy level splitting 20-70meV, hole levels spaced by ~10meV.
- Favourable for room temperature operation

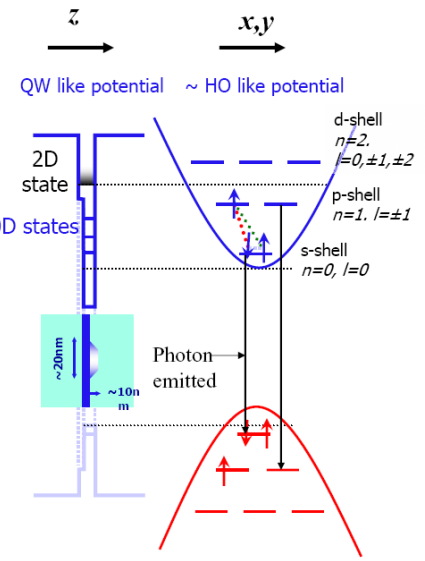

## Large Ensembles

**•Introduction to QD electronic structure, composition, shape**

**~$10^6$ – $10^7$ dots. Broadening due to shape and size fluctuations**

**The Quantum Confined Stark Effect**

## Optical Spectra

emission

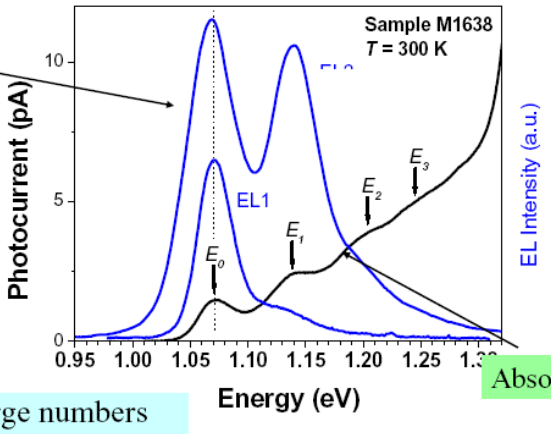


Absorption

Studies of large numbers ~$10^7$ dots.

Linewidth ~30meV due to shape and size fluctuations

# • Asymmetric Stark shifts

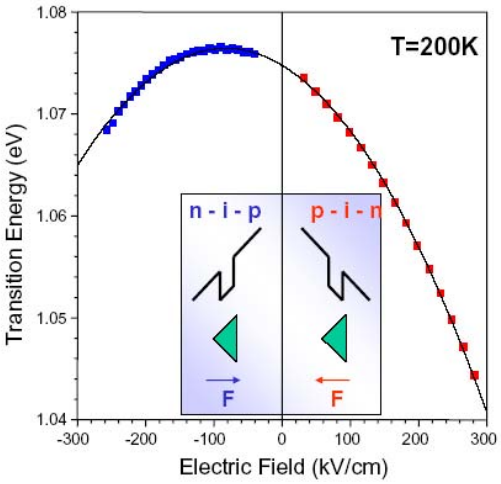


- Quadratic Stark shifts, $\Delta E$, asymmetric about zero field.

$$\Delta E = aF + bF^2$$

- Linear term implies existence of permanent dipole moment.

PRL 84, 733, 2000

From the sign of the dipole deduce that In composition increases from base to apex

Interdiffusion

**QDs are intermixed**

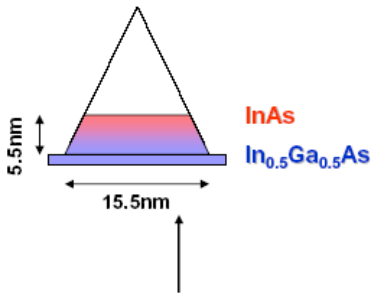


Increasing indium along growth direction

Polarisability - height

Theory, JA Barker and EP O'Reilly PR B61, 13840, 2000

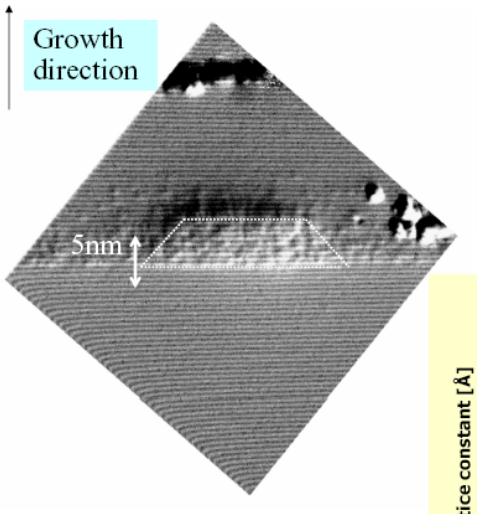


Truncated pyramid shape, In composition increases along growth axis

Scanning tunnelling microscopy

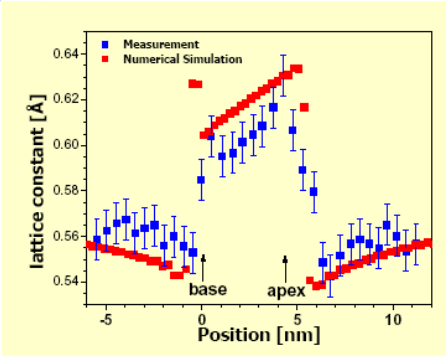


D Bruls, PM Koenraad, MSS et al
TU Eindhoven, **APL 81, 1708, 2002**

## Effects of Wavefunction Extent - Individual Quantum Dots

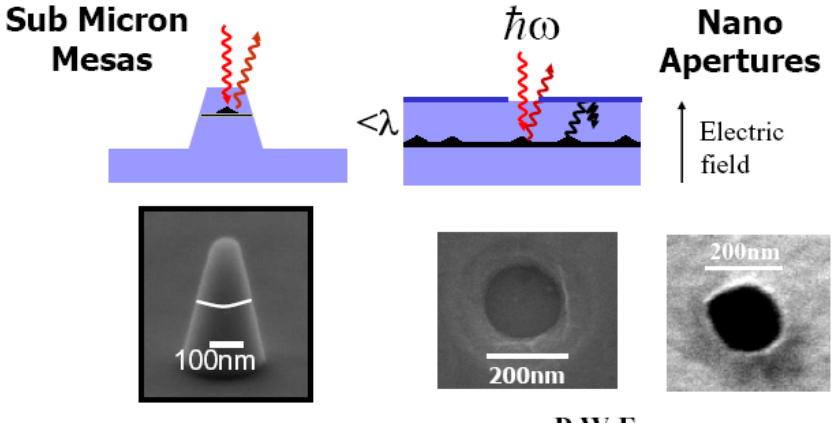


**P W Fry**

## Emission: Spatially resolved PL

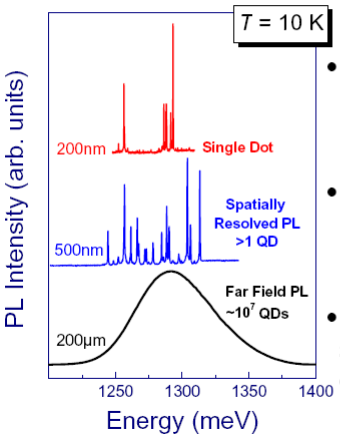


- Single dots may be optically isolated using apertures or mesas with ~2-500nm size.
- Emission spectrum breaks up into very sharp lines homogeneous linewidth ~ *1μeV*
- Ground (s-shell) and excited state (p-shell) emission observed

## Electron Charge Control, Single QDs

**Bester, Zunger PRB 67, 161306, 2003**

$X^-$ redshifted by ~5meV

2 electrons, one hole

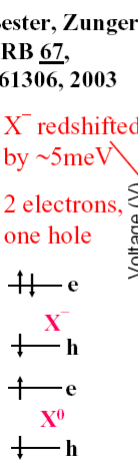


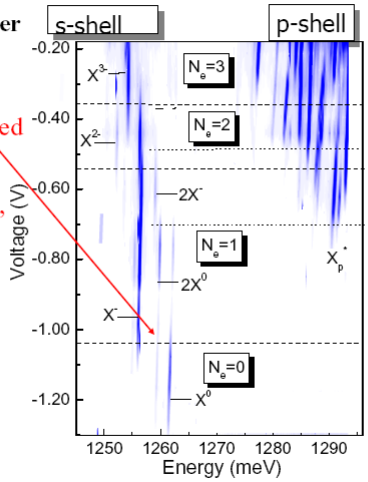


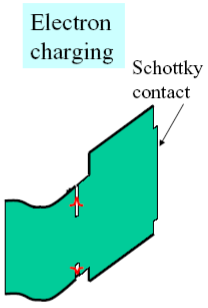


*Finley et al, PR B63, 073307, 2001, Warburton Nature 405, 926, 2000*

**Use electrons, eliminate excitonic recombination**

J. J. Finley et al, APL, 73, (1998) M. Kroutvar et al, APL 83 (2003)

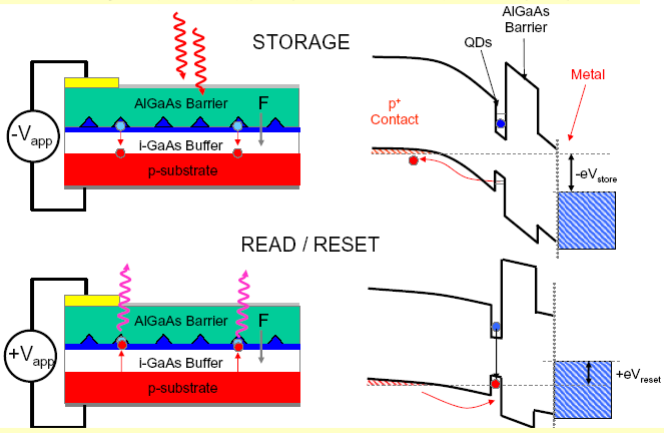


M Kroutvar, JJ Finley, G Abstreiter et al, TU Munich, Paper D1.004

1. Photocurrent, exciton created by resonant absorption, electron and hole tunnel out of dot and give current. Two step process.
2. Photoluminescence excitation spectroscopy. Three step process, absorption, relaxation and then recombination. Excited states. Coupling to environment.

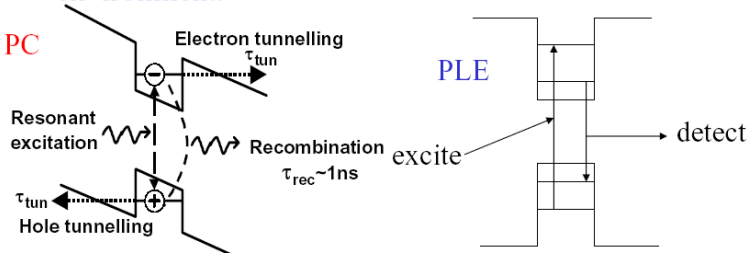

2. **Broad features in InAs-LO region. Indicate coupling to range of InAs-like phonons**
3. Resonant interaction at GaAs-LO energy

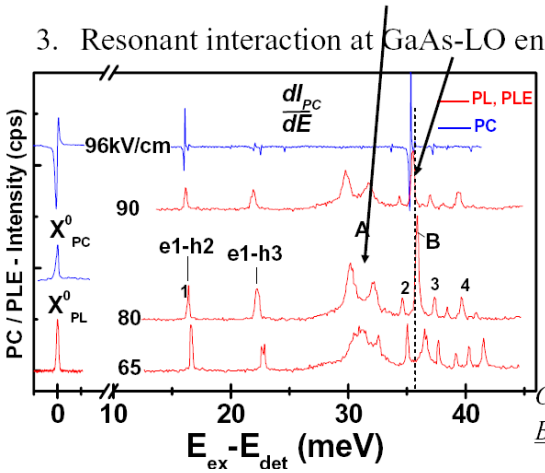


PLE

*Oulton et al, Phys Rev B68, 235301, 2003*

**To what extent do Stranski-Krastanow dots behave as atom-like systems**

1. Phonon coupling
2. Interaction with the Continuum (intrinsic). Probably undesirable

**Quantum dot and continuum transitions**

Quantum dot is not an isolated atom but is surrounded by 2D wetting layer quantum well and 3D GaAs

Atom-like system?

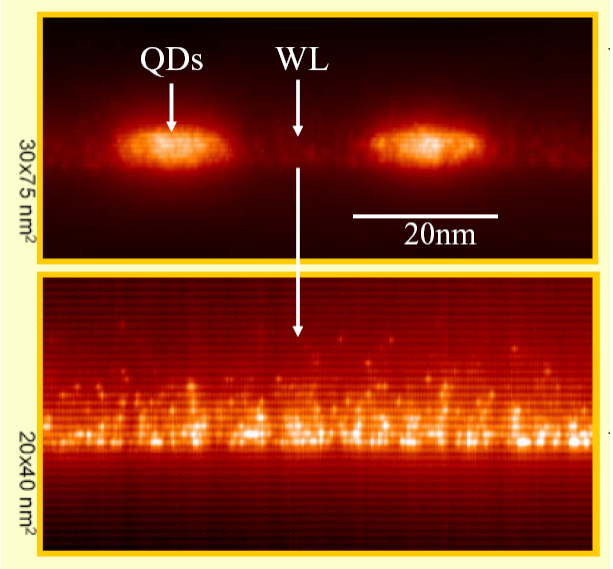


UHV-STM cross sections

PM Koenraad, TU Eindhoven

**Quantum dot/wetting layer energy level diagram**

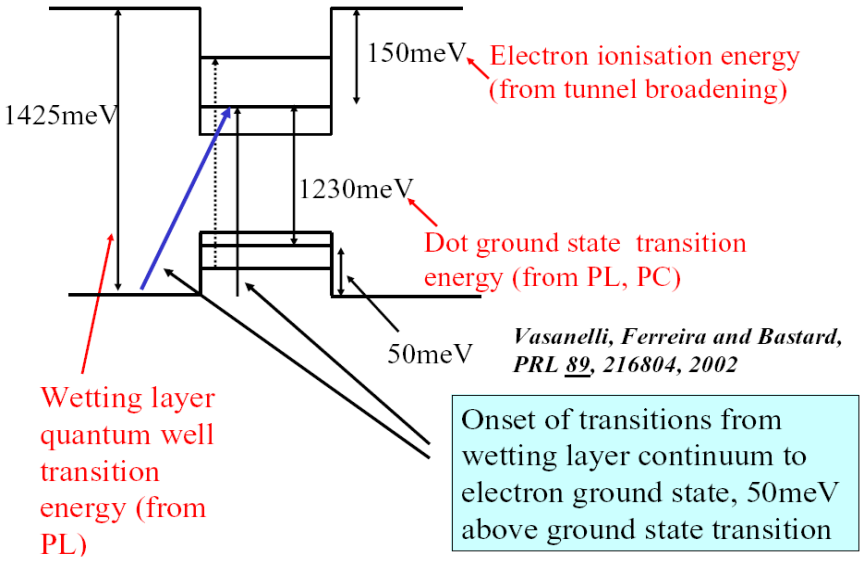


*Vasanelli, Ferreira and Bastard, PRL 89, 216804, 2002*

Onset of transitions from wetting layer continuum to electron ground state, 50meV above ground state transition

**Applications** (much physics as well!)

1. QD lasers
2. Mid infra-red detectors — Ensembles
3. Memory devices
4. Quantum information — Single dots
5. Single photon sources

QD lasers first discussed Arakawa and Sakaki, APL 40, 939 (1982)
*First report Kirstaedter, Bimberg et al, El Lett 30, 1416, 1994*

Low threshold, temperature insensitive threshold current etc

Breakthrough application, 1.3μm lasers for local area networks

Distinct potential advantages over installed InP-based lasers (GaAs-based technology, large area substrates, good thermal conductivity, Bragg mirrors, low temperature dependence of threshold current)

Major contributions, Berlin, Ioffe, New Mexico etc

## Semiconductor Laser Performance Versus Year

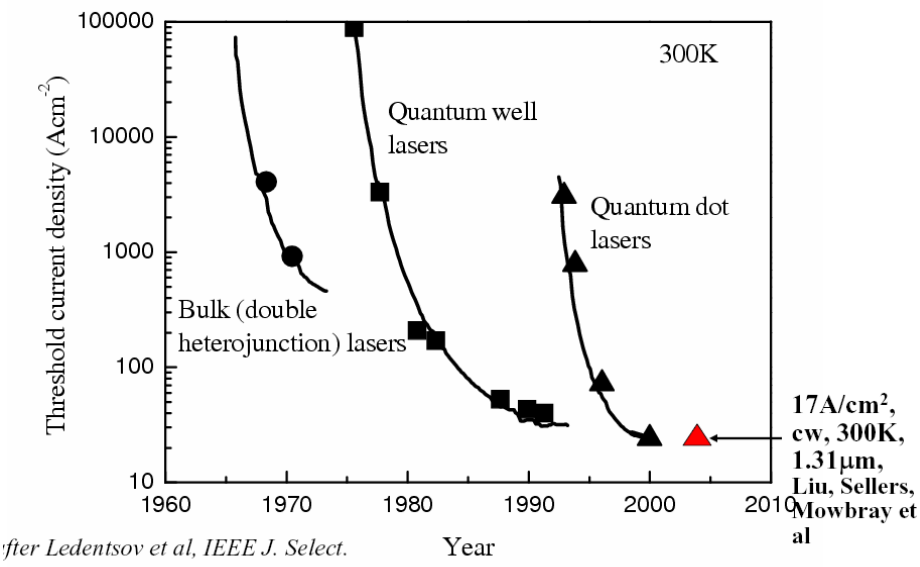


*after Ledentsov et al, IEEE J. Select. Topics Quant. Electron. 6, 439 2000*

## Dot in Well Structures (increase wavelength, but retain high density) - engineering of dot properties

1.3μm achieved with high density, good structural properties

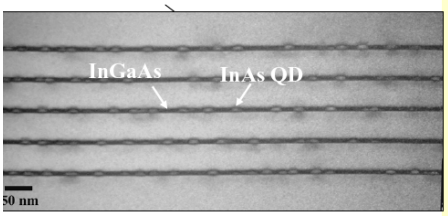


**DWELL structures**

- InAs dots in InGaAs wells
- Increases size of dots
- Reduces strain
- Enables 1.3μm
- High density ~ 3.5 x $10^{10}$cm$^{-2}$

See Liu et al, Appl Phys Lett, 26 July 2004 and paper J5.208

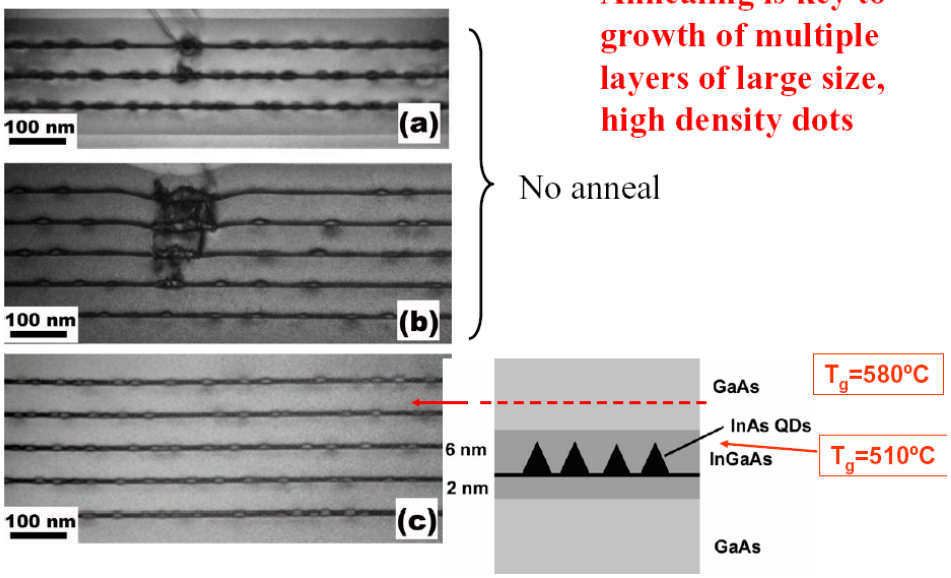


**Annealing is key to growth of multiple layers of large size, high density dots**

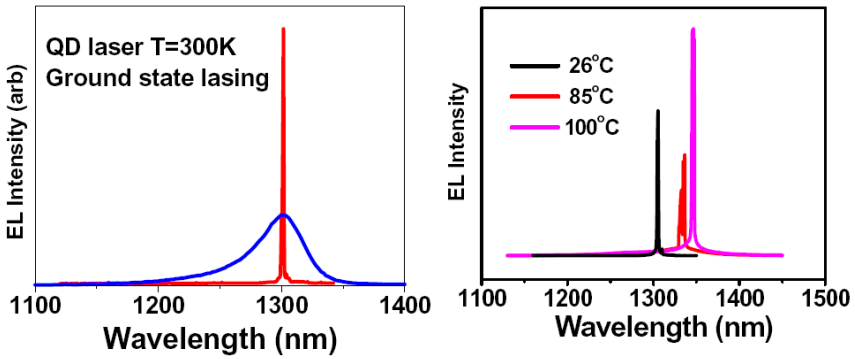


Record threshold currents, continuous wave 17A/cm$^2$ at 300K at true 1.3μm

Very encouraging temperature performance

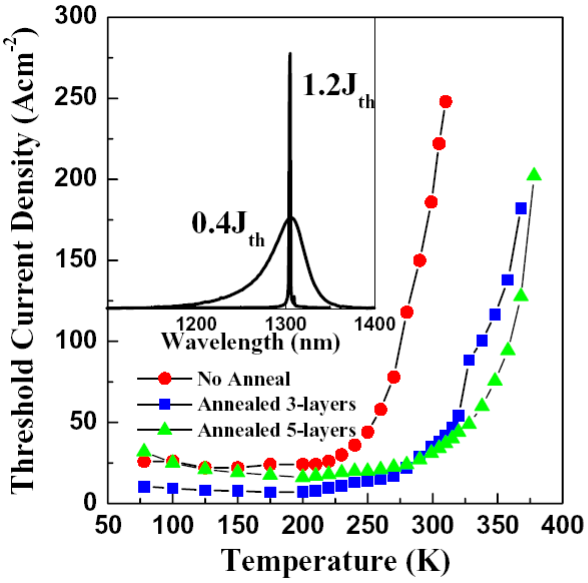


**Major improvement in threshold current with high T growth step**

**$J_{th}$ nearly independent of T up to 300K – characteristic of 0D density of states**

**Excellent Temperature Performance of 1.3μm QD lasers**

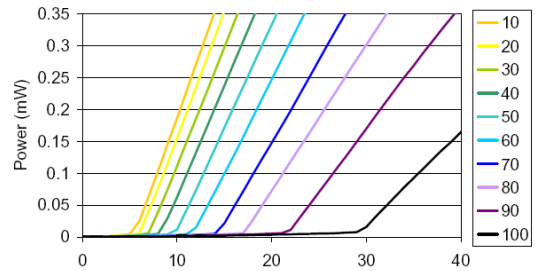


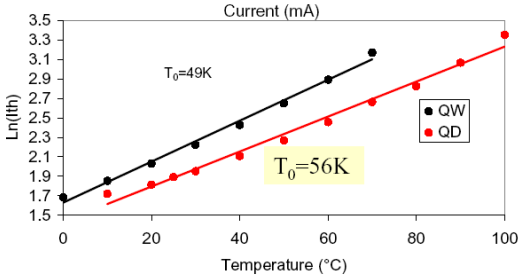


QD devices show excellent high T behavior with no significant increase in $T_0$ (56K) up to 100°C

Kovsh et al NSC-Nanosemiconductors $T_0$ ~ 150K up to 80°C)

*D Childs, Bookham, IR Sellers, KM Groom, DJ Mowbray, HY Liu, M Hopkinson*

## Long Lifetime Quantum Dot Lasers

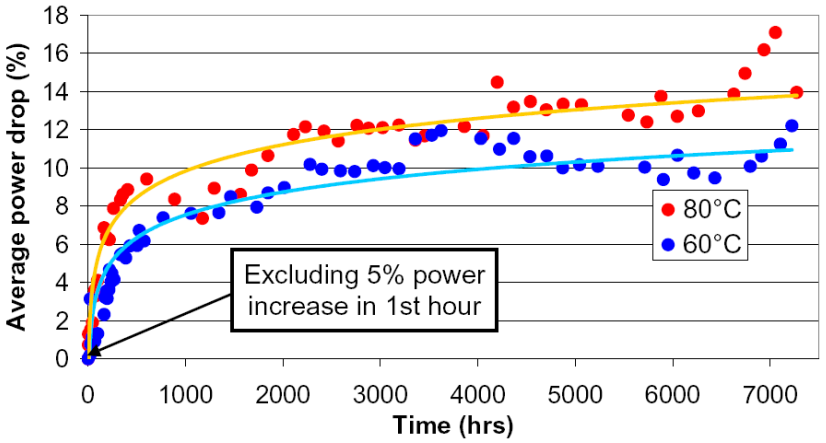


>4 years to 80% at 80°C (1500Acm$^{-2}$ )

>21 years to 80% at 60°C

Collaboration with

Bookham TECHNOLOGY

## QDs as Single Photon Sources

One photon emission per excitation pulse at defined energy. **Coulomb shifts enable**

- Exhibit photon antibunching, non-Poissonian light source. Non-classical light
- **Key component of quantum cryptography system**

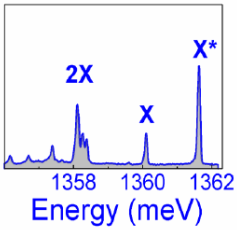


Michler et al Science 290, 2282, 2000, Moreau et al PRL 87, 183601, 2001, Yuan et al Science 295, 102, 2002

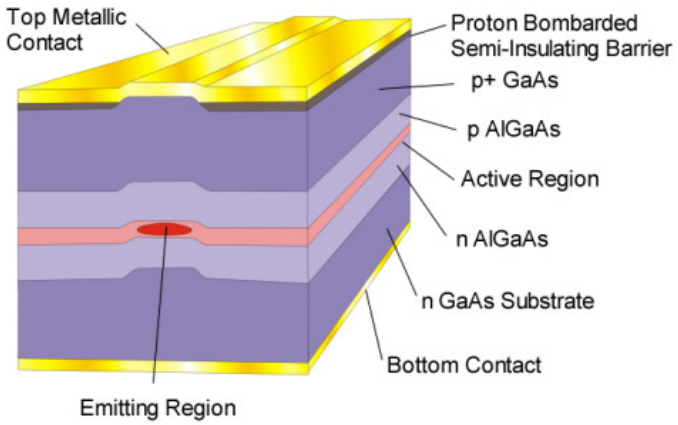


Britney Spears guide to Semiconductor physics
http://britneyspears.ac/lasers.htm

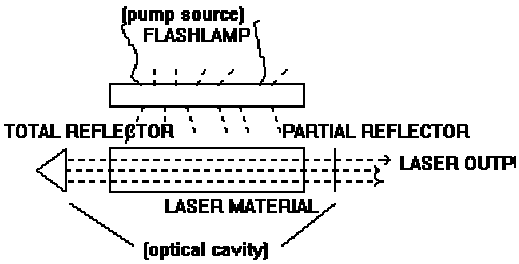


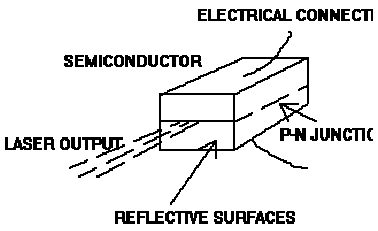


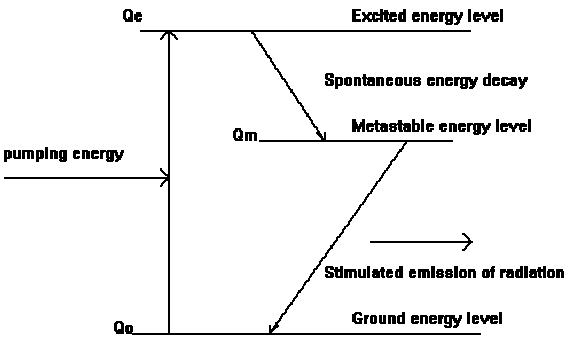

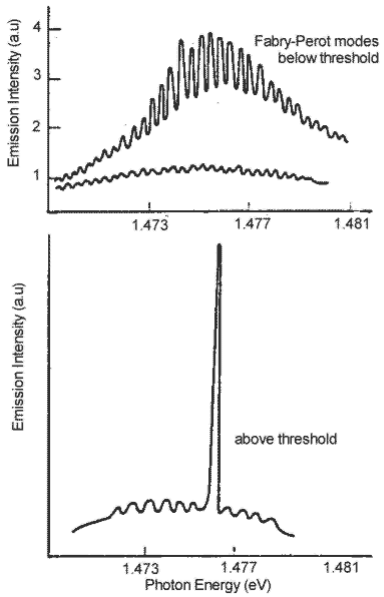
Emission Intensity (a.u)
4
3
2
1
Fabry-Perot modes
below threshold
1.473
1.477
1.481
Emission Intensity (a.u)
above threshold
1.473
1.477
1.481
Photon Energy (eV)

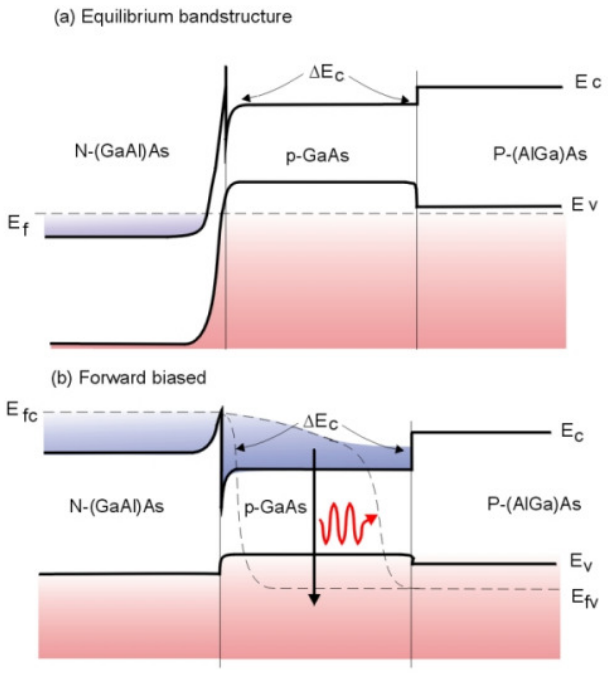
(a) Equilibrium bandstructure
ΔEc
Ec
N-(GaAl)As
p-GaAs
P-(AlGa)As
Ev
Ef
(b) Forward biased
Efc
ΔEc
Ec
N-(GaAl)As
p-GaAs
P-(AlGa)As
Ev
Efv

http://ece-www.colorado.edu/~bart/book/movie/movie5.htm
Semiconductor Laser
Photo Diode
Optoelectronic Transmitter and Reciever
Silicon MOSFET
Digital Light Projector
Cell Phone

# Photo Diode

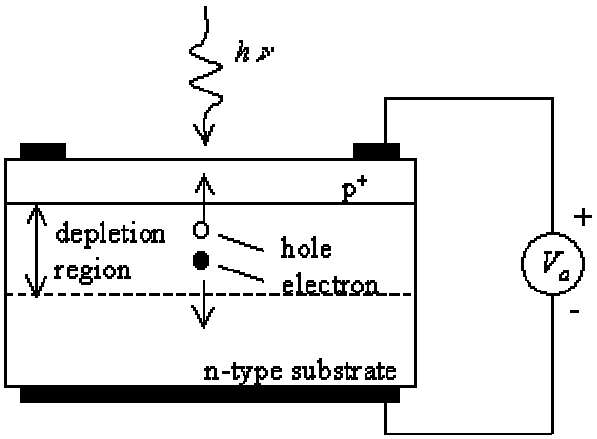


$$I = I_s(e^{V_a/V_t} - 1) - I_{ph}$$

$$I_{ph,max} = \frac{q}{h\nu} P_{in}$$

$$I_{ph} = (1-R)(1-e^{-\alpha d})\frac{qP_{in}}{h\nu}$$

# Solar Cell

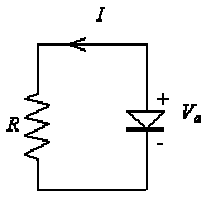


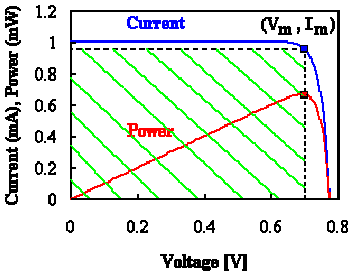


A 1 cm2 silicon solar cell has a saturation current of 10-12 A and is illuminated with sunlight yielding a short-circuit photocurrent of 25 mA. Calculate the solar cell efficiency.

The maximum power is generated for:

$$\frac{dP}{dV_a} = 0 = I_s\left(e^{V_m/V_t} - 1\right) - I_{ph} + \frac{V_m}{V_t} I_s e^{V_m/V_t}$$

Using iteration $V_m$ = 0.540 V and the efficiency equals:

$$\eta = \left|\frac{V_m I_m}{P_{in}}\right| = \frac{0.54 \times 0.024}{0.1} = 13\%$$

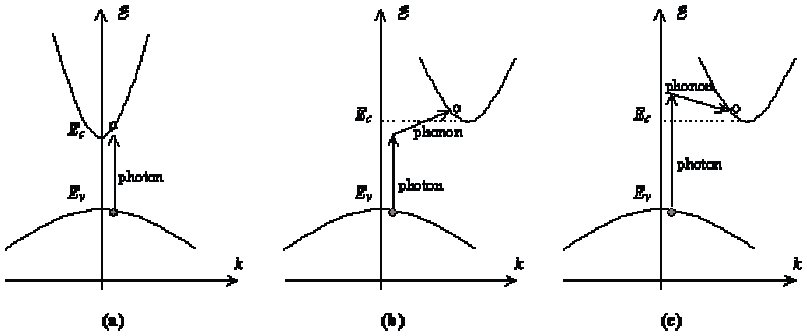


*E-k* diagram illustrating a) Photon absorption in a direct bandgap semiconductor b) Photon absorption in an indirect bandgap semiconductor assisted by phonon absorption and c) Photon absorption in an indirect bandgap semiconductor assisted by phonon emission.

Asryan and Suris, Int. J. High Speed Elec. and Sys. **12**, 111 (2002)

Issues:

Size Uniformity (etc.)
Recombination
Dot Density

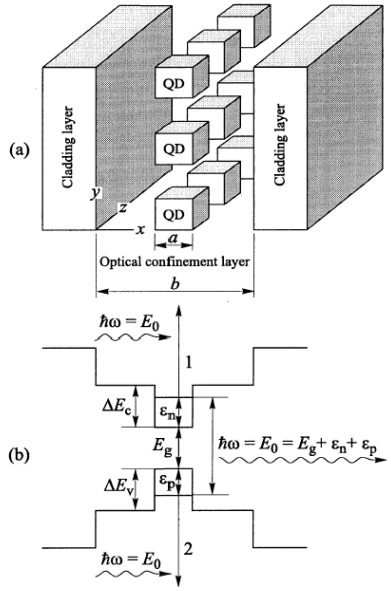


Fig. 1. Schematic (a) and energy band diagram (b) of a QD laser structure. The QDs are not drawn to scale. Arrows 1 and 2 show the transitions of carriers from the quantized energy levels to the continuous-spectrum states in the process of light absorption.

## Defect Reduction:

N.N. Ledentsov et al., Int. J. High Speed Elec. and Sys. **12**, 177 (2002)